CA, USA). Titanium concentration in blood and tissue samples as well as mouse diets (Oriental Yeast Co., ltd., Tokyo, Japan) was also determined using ICP-MS. In addition, a bibliographical search was done for the titanium concentration in foods, soil and others.

Preparation of titanium dioxide nanoparticles dispersed in saline

Titanium dioxide nanoparticles (MT-150AW, particle diameter of 15 nm, as explained below) were obtained from Tayca (Osaka, Japan). Highly dispersed titanium dioxide nanoparticles, HD-MT-150AW, were prepared by the following patented method for dense skins of hydrated amorphous silica bound to a core. MT-150AW (100 g) was mixed and well dispersed in 900 g of water, and then the pH of the mixture was adjusted to pH 9.0 by adding NaOH solution and the mixture heated to 80°C. Next, 200 g/l (as SiO_2) liquid glass (sodium silicate) (215 ml) and 10% H_2SO_4 (180 ml) were added to the mixed solution (ca. 1,000 g) and vigorously stirred for 2 hr (Iler, 1959). The final pH of the resultant mixture was adjusted to 8.0 to 8.5. Stirring was continued for another 30 min and then the pH of the solution was adjusted to 7.0 by addition of NaOH solution. Finally, the reaction mixture was filtered and 2,000 g of purified water was added to rinse. The solution was dried at 120°C for 12 hr and jet-milled to obtain HD-MT-150AW.

Titanium dioxide nanoparticles dispersed in physiological saline, DIS-HD-MT-150AW, were prepared by sonication of HD-MT-150AW. A mixture of 6 g of HD-MT-150AW and 54 g of physiological saline purchased from Sigma-Aldrich (St. Louis, MO, USA) was sonicated using a sterile ultrasonic grinding device (Ultrasonic Generator Model US-300, Nihonseiki Kaisha, Ltd., Tokyo, Japan) for 3 min under cooling conditions to obtain DIS-HD-MT-150AW.

Determination of physical and chemical properties of titanium dioxide nanoparticles

The silica content in HD-MT-150AW was analyzed using fluorescent X-ray spectroscopy (3270E, Rigaku Corp., Tokyo, Japan), and the crystal form of the nanoparticles was determined using X-ray diffraction (X'Pert Pro, PANalytical, Ea Almelo, Netherlands). The total number of bacteria in DIS-HD-MT-150AW was determined by a plate counting method.

The primary particle-size distribution of HD-MT-150A was analyzed using image processing software (MacView Ver. 3, Mountech Co., Ltd., Tokyo, Japan). The secondary particle-size distribution of DIS-HD-MT-150AW was determined using a dynamic light scattering particle-size analyzer (Microtrac 9340-UPA, Nikkiso Co., Ltd., Tokyo, Japan).

Intravenous administration of titanium dioxide nanoparticles

Male ddY mice weighing about 30 g were used in all animal experiments. These experiments were done under the guidelines of Life Science Research Center, Josai University. Saline suspension (50 μl) of titanium dioxide nanoparticles (DIS-HD-MT-150AW) (36,250 μg/ml, 1,813 μg/animal) was intravenously injected into the tail vein of mice under anesthesia by *i.c.* injection of sodium pentobarbital. The blood, brain, lung, heart, liver, spleen and kidney were excised 5 min, 72 hr and 1 month after injection. Tissue and blood were dissolved using Soluene-350 (Perkin-Elmer, Waltham, MA, USA) to determine the titanium concentration by ICP-MS, as explained above.

Morphological evaluation of excised tissues

Slices of the liver were observed by electron microscope (JEM2000EX, JEOL Ltd., Tokyo, Japan) to evaluate the intra- and inter-cellular presentation of titanium dioxide nanoparticles.

RESULTS AND DISCUSSION

Survey of titanium concentration in typical food materials

As described in the Introduction, titanium is naturally contained in several vegetables and soil, although there is no detailed information on the chemical structure of the compounds. The titanium level in several foodstuffs was therefore determined and a brief survey was carried out on several food materials; Table 1 summarizes these surveys and the experimental results. An unexpectedly high titanium concentration was observed in several food materials. In particular, the titanium concentration in soybeans (3.24 μg/g) and shrimp (2.52 μg/g) was high. Itoh *et al.* (2005) reported that the titanium concentration in several soils was over 3,300 μg/g, which may be related to the relatively high concentration in vegetables (*i.e.*, 20-30 μg/g for Chinese cabbage).

Preparation and characterization of titanium oxide nanoparticles

The preparation and physical properties (size) are very important for the safety and toxicity of titanium dioxide nanoparticles. Titanium dioxide nanoparticles dispersed in physiological saline, DIS-HD-MT-150AW, were prepared using the following two steps: preparation of highly dispersed titanium dioxide nanoparticles, HD-MT-150AW

Table 1. Titanium level in several foodstuffs and others

Food/Soil	Production area	Conc. (μg/g)	Food/Soil	Production area	Conc. (μg/g)
beef	Japan	0.17	lettuce [a]		41 ± 15
beef	Australia	0.26	Boston lettuce [a]		10 ± 14
pork	Japan	0.26	Japanese parsley [a]		53 ± 12
pork	USA	0.44	Japanese radish (leaf) [a]		37 ± 33
chicken	Japan	0.14	Welsh onion [a]		20 ± 13
egg	Japan	1.70	tomato [a]		39.1 ± 9.2
salmon	Norway	0.37	paprika [a]		14 ± 16
shrimp	India	2.52	sprout [a]		38 ± 16
onion	Japan	0.33	AIN 93G [b]	Josai Univ.	6.29
potato	Japan	0.12	α cornstarch		0.18
paprika	Netherlands	0.19	β cornstarch		0.18
carrot	USA	0.59	casein		1.60
corn	USA	0.60	cellulose		< 0.1
flour	mainly USA	0.31	soft water	USA	< 0.05
soybeans	Japan	3.24	water	Thailand	< 0.05
rice	Japan	0.91	soft water	France	< 0.05
orange	USA	0.65	mid-hard water	France	< 0.05
lemon	USA	1.64	hard water	France	< 0.05
grapefruit	South Africa	0.39	urban water	Thailand	< 0.05
banana	Philippines	< 0.1	soft water	Japan	< 0.05
Japanese parsley [a]	Japan	101 ± 19	soft water	Japan	< 0.05
Japanese parsley [a]	Japan	10 ± 13	water [a]	Japan	13 ± 17 (ng/g)
Chinese cabbage [a]	Japan	29.5 ± 14	water [a]	Japan	3.2 ± 8.0 (ng/g)
Chinese cabbage [a]	Japan	20 ± 13	soil [a]	Japan	4980 ± 220
bok-choy [a]		35.0 ± 8.8	soil [a]	Japan	3380 ± 180
Chinese cabbage [a]		22 ± 19	soil [a]	Japan	5540 ± 230
Cabbage [a]		52.7 ± 11	soil [a]	Japan	5870 ± 260
Macrophyll [a]		12.0 ± 6.0			

[a] Itoh *et al.* (2005), [b] from Prof. Wada (Josai Univ.)

from MT-150AW, and dispersion of HD-MT-150AW in saline by sonication to obtain DIS-HD-MT-150AW.

The surface of HD-MT-150AW was coated with silica. The isoelectric point of titanium dioxide is about 5-7, so titanium dioxide nanoparticles (MT-150AW) dispersed in physiological saline can be easily agglomerated. In other words, the surface modification of MT-150AW to HD-MT-150AW by silica was effective to avoid agglomeration in neutral saline, because the isoelectric point of silica is about 2-3.

The silica content of HD-MT-150AW analyzed by fluorescent X-ray spectroscopy was 27.5 wt%. X-ray diffraction patterns of HD-MT-150AW showed that the crystal form of titanium dioxide was rutile (data not shown). No bacteria were detected in DIS-HD-MT-150AW, as determined by the plate counting method.

Fig. 2 shows transmission electron microscope images of MT-150AW and HD-MT-150AW. Fig. 1 illustrates the grading curve of HD-MT-150AW, showing that it had a relatively narrow primary particle-size distribution and a mean particle diameter of 15 nm.

Fig. 3 shows the grading curve of the particles in DIS-HD-MT-150AW. The secondary particle-size distribution was wide, with an average particle size of 0.22 μm (220

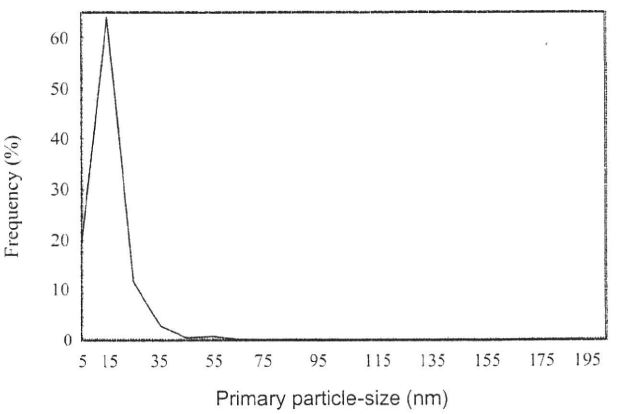

Fig. 1. Primary particle-size distribution of HD-MT-150AW analyzed by image processing software

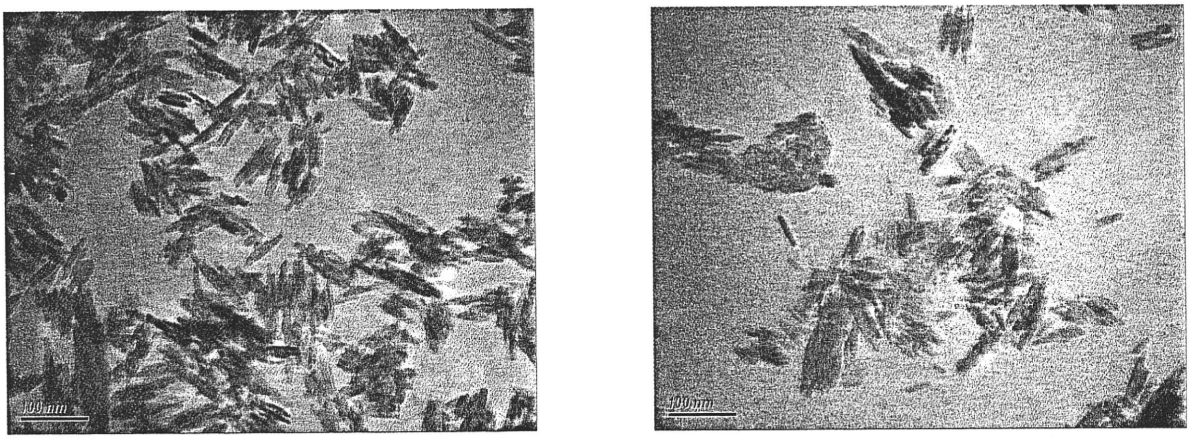

Fig. 2. Transmission electron microscope image of MT-150AW and HD-MT-150AW
Left side: MT-150AW, Right side: HD-MT-150AW .

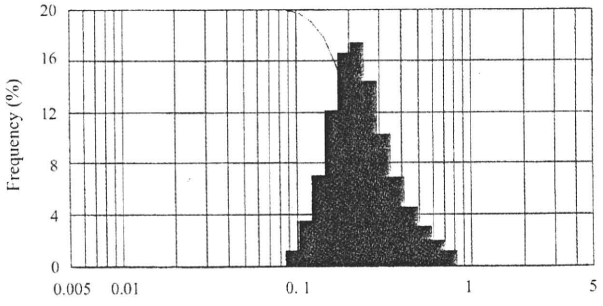

Fig. 3. Grading curve of particles in DIS-HD-MT-150AW analyzed by dynamic light scattering particle-size analyzer

nm). Fig. 3 shows that DIS-HD-MT-150AW contains only a small number of particles with a particle diameter below 100 nm. Fig. 4 shows a transmission electron microscope image of DIS-HD-MT-150AW particles. DIS-HD-MT-150AW clearly contained the primary particles of HD-MT-150AW.

Tissue distribution of titanium after *i.v.* injection of titanium dioxide nanoparticles

Titanium was detected in the blood and tissue of healthy mice without the administration of titanium dioxide nanoparticles, and the titanium levels are shown in Figs. 5 and 6 (see blank column for control). For example, titanium concentrations in the blood and liver were 4 and 15.4 μg/g tissue, respectively. Then, the titanium level was determined in the mouse diets and was found to be 17.5 μg/ml. Since the experimental animals consume about 5 g solid feed per day, the amount of titanium ingested was calculated to be 90 μg/day. Thus, most titanium in mice must come from ingested titanium materials.

Forced *i.v.* injection of the nanoparticles was then performed in mice. The titanium level was significantly increased in blood and tissue, but no increase was found in the brain after *i.v.* injection. No increase in the brain level may ignore the severe toxicity reported by Long *et al.* (2007). Most titanium was concentrated in the liver after injection, followed by the kidney as shown in Figs. 5 and 6. Interestingly, the liver level decreased over time (ca 30% decrease in 1 month), suggesting that titanium must be eliminated from the body. Fig. 7 shows the total recovery of titanium from the tissues. The titanium lev-

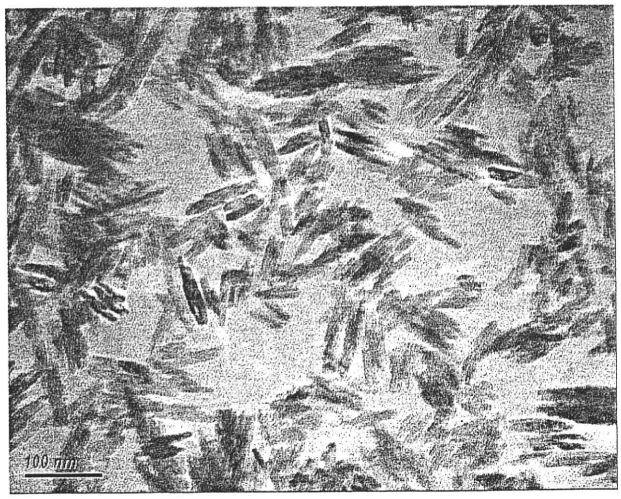

Fig. 4. Transmission electron microscope image of DIS-HD-MT-150AW

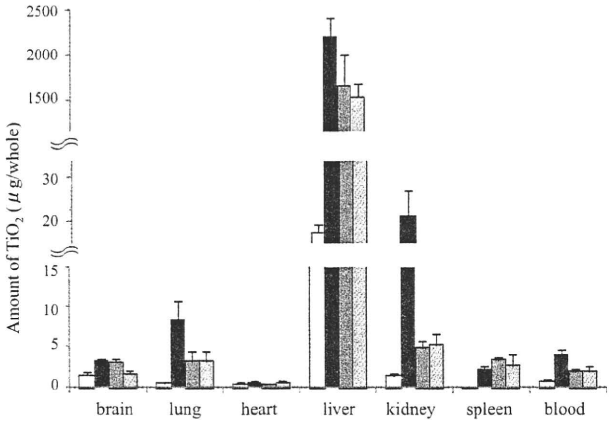

Fig. 5. Amount of TiO_2 in tissue and blood after *i.v.* injection
□ : before injection (control), ■, ▥ and ▤: 5 min, 72 hr and 1 month after injection. Each column represents the mean ± S.E. of 3 to 5 experiments.

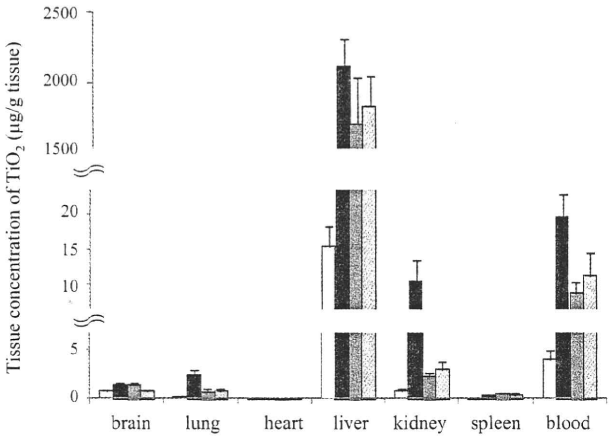

Fig. 6. Tissue concentration of TiO_2 after *i.v.* injection
Each column is the same as in Fig. 5.

el in mice apparently decreased over time after injection. Recently, a similar *i.v.* injection study of titanium dioxide nanoparticles was performed in rats by Fabian *et al.* (2008), where titanium was mostly detected in the liver and decreased over time. Jani *et al.* (1994) showed the distribution of orally administered titanium dioxide particles (100-500 nm) in the liver and spleen. Dental implants made of titanium were found to dissolve in biological tissues and were not toxic (Mu *et al.*, 2002; Hanawa, 2005). Their and our results suggest that titanium dioxide nanoparticles should be considered as a biodegradable or easily eliminated compound, not like asbestos and carbon nanotubes.

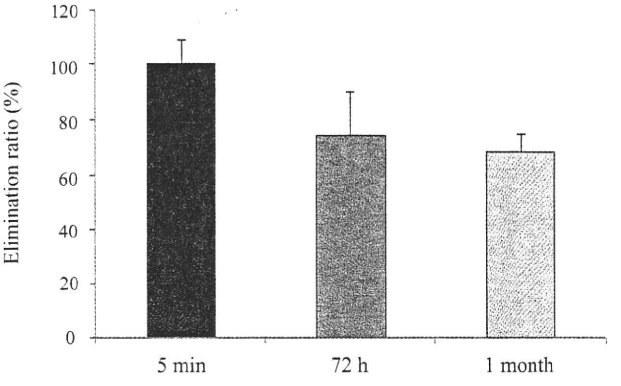

Fig. 7. Elimination ratio of TiO_2
Each column represents the mean ± S.E. of 5 experiments.

Finally, morphological evaluation was performed in mouse liver after administration of titanium dioxide nanoparticles, which were observed in hepatic cells. Titanium dioxide nanoparticles may be dissolved by macrophagic activity in the liver (Olmedo *et al.*, 2007). Detailed information will be presented in a separate paper.

Titanium was naturally contained in mice, especially in the liver, as well as in vegetables and soil. The titanium level gradually decreased after forced administration (*i.v.* injection) of titanium dioxide nanoparticles into mice. Thus, our strategy to estimate the safety of titanium dioxide nanoparticles in humans must be modified, although further experiments are necessary (Behling, 2007).

REFERENCES

Behling, B. (2007): EC committee proposes new nanomaterials risk assessment procedure. The Rose Sheet, **28**, 12.

Fabian, E., Landsiedel, R., Ma-Hock, L., Wiench, K., Wolleben, W. and van Ravenzwaay, B. (2008): Tissue distribution and toxicity of intravenously administered titanium dioxide nanoparticles in rats. Arch. Toxicol., **82**, 151-157.

Hanawa, T. (2005): Surface treatment of titanium in medical applications. Journal of Japan Institute of Light Metals, **55**, 553-556.

Iler, R.K., (1959): U. S. Patent, No.2885366.

Itoh, J., Saitoh, Y., Futatsugawa, S. and Sera, K. (2005): Elemental analysis of the vegetables on the market; Comparison with wild plants. NMCC Annual Report, 13.

Jani, P.U., McCarthy, D.E. and Florence, A.T. (1994): Titanium dioxide (rutile) particle uptake from the rat GI tract and translocation to systemic organs after oral administration. Int. J. Pharm., **105**, 157-168.

Lomer, M.C., Hutchinson, C., Volkert, S., Greenfield, S.M., Catterall, A., Thompson, R.P. and Powell, J.J. (2004): Dietary sources of inorganic microparticles and their intake in healthy subjects and patients with Crohn's disease. Br. J. Nutr., **92**, 947-955.

Long, T.C., Tajuba, J., Sama, P., Saleh, N., Swartz, C., Parker, J., Hester, S., Lowry, G.V. and Veronesi, B. (2007): Nanosize titanium dioxide stimulates reactive oxygen species in brain microglia and damages neurons *in vitro*. Environ. Health Perspect., **115**, 1631-1637.

Maynard, A.D., Aitken, R.J., Butz, T., Colvin, V., Donaldson, K., Oberdörster, G., Philbert, M.A., Ryan, J., Seaton, A., Stone, V., Tinkle, S.S., Tran, L., Walker, N.J. and Warheit, D.B. (2006): Safe handling of nanotechnology. Nature, **444**, 267-269.

Mu, Y., Kobayashi, T., Tsuji, K., Sumita, M. and Hanawa, T. (2002): Causes of titanium release from plate and screws implanted in rabbits. J. Mater. Sci. Mater. Med., **13**, 583-588.

Olmedo, D.G., Tasat, D.R., Evelson, P., Gulielmotti, M.B. and Cabrini, R.L. (2008): Biological response of tissues with macrophagic activity to titanium dioxide. J. Biomed. Mater. Res. A., **84**, 1087-1093.

Scientific Committee on Consumer Products (2007): Preliminary opinion on safety on nanomaterials in cosmetic products.

Scientific Committee on Emerging and Newly-Identified Health Risks (2007): Opinion on the Appropriateness of the risk assessment methodology in accordance with the technical guidance documents for new and existing substances for assessing the risk of nanomaterials.

Singh, R., Pantarotto, D., Lacerda, L., Pastorin, G., Klumpp, C., Prato, M., Bianco, A. and Kostarelos, K. (2006): Tissue biodistribution and blood clearance rates of intravenously administered carbon nanotube radiotracers. Proc. Natl. Acad. Sci. USA., **103**, 3357-3362.

Erratum

Safety evaluation of titanium dioxide nanoparticles by their absorption and elimination profiles

Kenji Sugibayashi, Hiroaki Todo and Eriko Kimura
J. Toxicol. Sci., **33**, 293-298 (2008).

[Page 293, right side line 9]
Error:
titanium oxide

Correction:
titanium dioxide

[Page 296, left side line 13-14]
Error:
titanium concentrations in the blood and liver were 4 and 15.4 μg/g tissue

Correction:
titanium concentrations in the blood and liver were 0.7 and 14.4 μg/g tissue

[Page 296, left side line 16]
Error:
17.5 μg/mL

Correction:
17.5 μg/g

[Page 296, right side line 9-10]
Error:
after injection, followed by the kidney as shown in Figs. 5 and 6.

Correction:
after injection as shown in Figs. 5 and 6.

[Fig. 5]
Error:

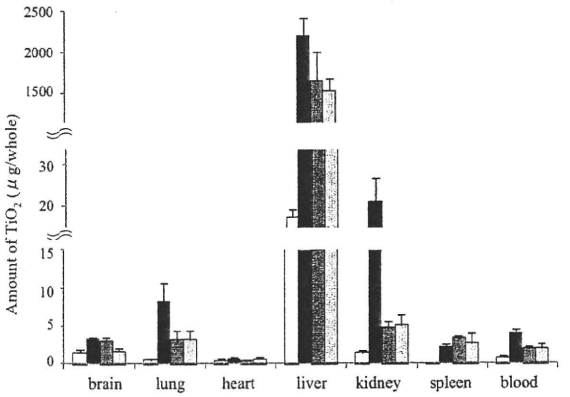

Correction:

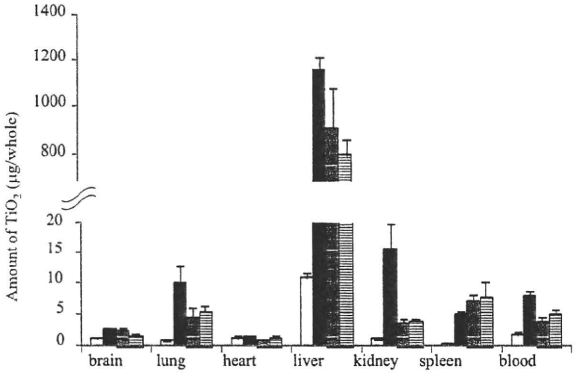

[Fig. 6]
Error:

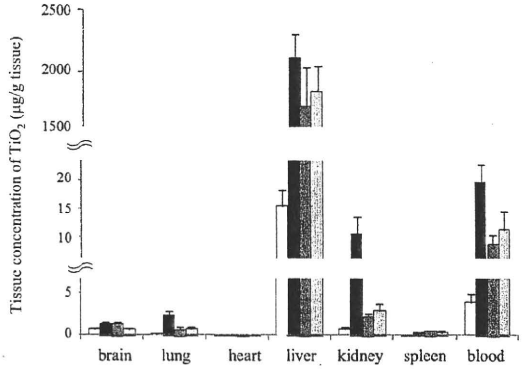

Correction:

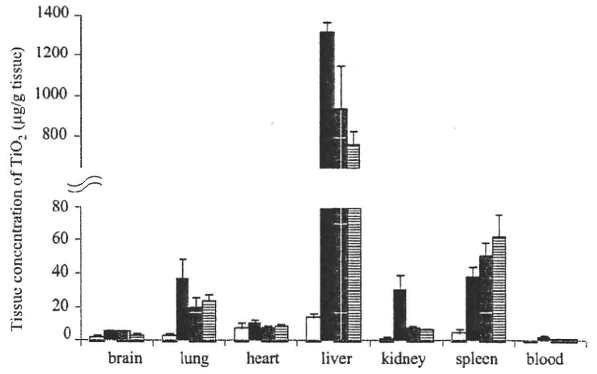

化粧品に用いられるナノ粒子の暴露と安全性問題のあり方

杉林 堅次

Abstract : It is an urgent problem to evaluate safety concern of nanomaterials such as titanium oxide- and zinc oxide-nanoparticles that are broadly used as an UV-scattering cosmetic. The primary diameter of the nanomaterials is 15-50 nm. Possible exposure sites to human are the GI tracts, respiratory tracts (nasal cavity, trachea, tracheal branch and alveolus of the lung) and skin. Skin must be most important exposure site among them especially for general consumers. As easily understood by the 500 Dalton rule (where these small molecules have 0.2-0.4 nm in diameter), nanomaterials are hardly penetrated into the skin tissues through stratum corneum, primary permeation pathway of most compounds. We have to pay attention to the second permeation pathway (transfollicular pathway) of skin entry in case of nanomaterials. We also consider several wound skins which have low skin barrier function compared with normal skin for nanomaterial penetration into skin. In addition, we must consider the nanomaterial exposure in a quantitative way not qualitative way. For example, the resquamation rate and permeability coefficient of water are 1×10^{-9} and 2×10^{-7} cm/s, respectively. Physicochemical properties of nanomaterials are also important determinants for their skin entry.
Evaluation study on the nanomaterial safety is just the mark of the start line. We have to pay attention to this issue.

Key words : nanomaterial, safety, skin exposure, titanium oxide nanoparticle, zinc oxide nanoparticle, 500 Dalton rule, permeability coefficient

1. はじめに

地球上に生活する我々人類に大きな影響を与える紫外線はその波長によりUVA（紫外線A波），UVB（紫外線B波）およびUVC（紫外線C波）に分けられる。これらのうち，一番短波長域にあり地上には到達しないUVCには殺菌効果があり，UVBにはビタミンDの生合成を助ける有用な働きがある。その一方で，UVBは表皮に侵入してサンバーン（赤い水ぶくれのような状態）と言われる肌の炎症を引き起こし，加えて，直接的に，また，間接的に活性酸素を介して，表皮細胞中のDNAを損傷させる。重篤な場合，これらは表皮細胞の細胞死や皮膚癌の原因にもなる。特に，近年のオゾン層破壊による皮膚癌発生率の増加は紫外線照射による有害事象として注目すべきである。さらに，UVAは表皮のメラノサイトを刺激して，肌の色を黒くするサンタン（日やけ）を招く。サンタン自体は肌を守る作用があるものの，UVAの半分は皮膚深部（真皮）にまで到達して，肌のハリを支えているコラーゲン架橋結合を破壊してシワの原因になる。

紫外線防御化粧品（UVケア化粧品）は，この

"Margin of safety and exposure of nanomaterials used in cosmetics."

Kenji Sugibayashi (Faculty of Pharmaceutical Sciences, Josai University, 城西大学薬学部薬粧品動態制御学講座— 350-0295 埼玉県坂戸市けやき台 1-1)

1985年城西大学薬学部講師，89年同助教授，98年同教授，現在，城西大学薬学部薬粧品動態制御学講座教授，同生命科学研究センター所長，薬科学科主任。日本香粧品科学会理事，日本実験動物代替法学会評議員，他。

ような人体（特に肌）に悪い影響を与える紫外線(UVA, UVB）から肌を守るために極めて有用であり，化粧品としての価値だけでなくヘルスケアにも対応できる医薬部外品になる。特に，UVケア化粧品のうち日やけ止め化粧品に，紫外線散乱剤として粒子径が15～50 nmの無機（酸化チタンや酸化亜鉛）超微粒子（ナノ粒子）が紫外線吸収剤と併用され始めるようになって，肌への紫外線防御効果が著しく高まった。

一方で，極めて細い繊維状物質でひとつのナノ材料あるアスベスト（石綿）の吸入によって肺線維症や肺癌，さらには稀な腫瘍である悪性中皮腫の危険性が大きく増すことが社会問題になった。また，この事件を契機にして，社会で広く使われているナノ材料・ナノ粒子の安全性を根本から見直すべきであるとの機運が高まった。酸化チタンや酸化亜鉛微粒子といったナノ粒子は皮膚から吸収されないと考えられて化粧品に含有された経緯があるが，アスベスト問題が浮上してから，酸化チタンや酸化亜鉛微粒子の安全性ももう一度根本から見直す必要がある。

2. ナノ材料の安全性

ナノ材料，特に紫外線防御剤のヒトへの安全性は，暴露部位を中心に考えていくべきであろう。表1に化学物質の暴露部位とその特徴をまとめて示す。すなわち，ナノ材料（紫外線防御剤）のヒトへの暴露経路としては，消化管，気道（鼻粘膜，気管・気管支，肺胞），そして皮膚が考えられる。表に示したように，紫外線防御剤を中心に考えれ

表1　ナノ材料（紫外線防御剤）の暴露部位とその特徴

暴露部位		特　徴	備　考
消化管（口，胃，小腸など）		経口暴露。乳児などは小腸にパイエル板（Payer's patch）が発達しており，高分子も吸収される可能性がある。	紫外線防御剤の誤用による暴露が考えられる。
気道	鼻粘膜	一般的に鼻呼吸において，粒径が2～20 μmの粒子では90％が鼻腔内に捕捉（暴露）される。鼻粘膜にはmucociliary clearanceという異物排除機能がある。鼻から脳へ直接物質が移行することがありうる。	肌に適用した紫外線防御剤が乾燥し，経気道暴露に至る可能性がある。ナノ材料を扱う作業労働者に対する危険性も考慮する必要があろう（肺胞はアスベストの最も重要な暴露経路であった）。
	気管・気管支	一般的に鼻呼吸において，粒径が1～5 μmの粒子では約50％が気管気管支領域に留まるが，10～20 μmの粒子が気管・気管支まで達することは少ない。一方，口呼吸においては，10～20 μmの粒子の95％以上が気管気管支に沈着し，1～10 μmの粒子の約60～80％は細気管支レベルに沈着する。気道への沈着は粒子の性状，気道の解剖学的要因，呼吸パターンに依存している。また，気道，肺胞腔内に沈着した粒子状物質は粘液線毛上皮系を主体とするクリアランス機構によって，その多くは排除される。	
	肺　胞	一般的に鼻呼吸において，1～5 μmの粒子の50％は肺胞領域に達するが，10 μm以上の粒子は肺胞レベルには沈着しない。一方，口呼吸においては，1～5 μmの粒子の40～50％は肺胞に沈着する。	
皮　膚		物質の経皮吸収の最大のバリアーである角層は大きな分子は通さない。毛嚢経路でどの程度の分子が皮膚中に侵入するか検討が必要。また，皮膚に傷がある場合は，ナノ材料がその部分から深部に侵入する可能性がある。	紫外線防御剤の暴露経路としては最も重要。

ば，その暴露経路の中心は経皮暴露であると考えられる。化粧品に含まれるナノ粒子ははたして皮膚中に滲入していくのか。

3. 物質の経皮吸収性と分子サイズ

物質のサイズ（分子量や分子容）と経皮吸収性の関係については，すでに本誌既刊号で考察したので，ここではその一部分だけを紹介する[1]。Bos と Meinardi は「分子量 500 ダルトン限界説（500 Dalton rule）」を報告している[2]。彼らは，現在までに皮膚感作性を示す物質の分子量のほとんどが 500 ダルトン以下であること，また，皮膚組織に薬物を送達する局所作用を期待する医薬品製剤やまた全身吸収性を期待した TDDS（Transdermal Drug Delivery Systems）中に含まれる薬物はほとんどが分子量 500 ダルトン以下であることを基準としてこの経験説を提唱している。すなわち，分子量 500 ダルトン以上の物質は皮膚を透過しないということである。分子量 500 ダルトン程度の物質の直径（または長径）は 0.2-0.4 nm 程度であるのに対し，今回問題にしている紫外線防御剤中のナノ材料は 15～50 nm の微粒子粉体であることを考え合わせると，100 倍程度の粒子径を有しているこれらナノ粒子は，常識から考えると皮膚から吸収することはほとんど不可能であると思われる。

しかし，皮膚には 500 ダルトン以下の物質の主透過経路である角層に加えて，毛嚢や汗腺といった付属器官が存在するため，ナノ材料のこれら付属器官を介した侵入の可能性についても検討する必要性がある。また，アトピー性炎症を呈する皮膚をはじめとしてバリアー能が著しく低下した皮膚や，傷を有した皮膚も対象にする必要があるなら，ナノ材料の皮膚透過性に及ぼす皮膚疾患や傷の影響についても評価しておく必要もあろう。

すでに本誌で考察した皮膚浸透経路に関する記述と，皮膚が溶解拡散膜なのか細孔膜なのかについての議論[1]についても正確に理解してナノ材料の安全性について考察していかねばならない。

4. 経皮吸収の定量的理解について

科学の著しい発達につれて，微量の物質を定量できる測定機器が開発され，物質の定量感度が上昇した。今まで測定限界以下であった物質が皮膚中に見られるようになると，不思議なことに，「皮膚に浸透しない物質」から「皮膚に浸透する物質」に表現法が変わる。まったく節操ないことで，科学に携わっている者からみると残念でならない。これは定量（程度）の概念が一般消費者だけでなく，科学者や科学・技術情報担当者にないためである。

皮膚浸透性や皮膚透過性の定量的指標として透

表２　種々物質の皮膚透過係数と皮膚透過係数の指標

透過係数 (cm/s)	指　標　と　特　徴
1×10^{-9}	角層一層の剝がれる（ターンオーバー）速度 1日で角層1層に浸透する速度
4×10^{-9}	クロモグリク酸ナトリウムのヘアレスラット皮膚透過係数
5×10^{-9}	カルセインナトリウムのヘアレスラット皮膚透過性
2×10^{-8}	1日で角層全層（20 μm）に浸透する速度
2×10^{-7}	水分子のヒトおよびヘアレスラット皮膚透過速度
	5－フルオロウラシルのヘレスラット皮膚透過速度
	ジクロフェナク酸ナトリウムのヘアレスラット皮膚透過速度
3×10^{-7}	皮膚を擦っても消えないボールペンやマジック色素の透過速度*
1×10^{-7}	ISMN のヒトおよびヘアレスラット皮膚透過係数
3×10^{-6}	ISDN のヒトおよびヘアレスラット皮膚透過係数
1×10^{-5}	リドカインのヒトおよびヘアレスラット皮膚透過係数
2×10^{-5}	5－フルオロウラシルのヘレスラット stripped skin 透過速度
1×10^{-4}	フルルビプロフェンやイブプロフェンのヘアレスラット皮膚透過係数

* 角層の5層目に入れば消えないと仮定

過係数（permeability coefficient, P, cm/s）が用いられる。角層は部位によって異なるが，約20層の角質細胞層からなり，約20 μmの厚みがある。最上層から1日1層剝がれるので，1 μm/day，すなわち，10^{-9} cm/s以下の透過係数を示す物質は，まる1日かかってようやく角層2層目直前に移行したとしても，このとき物質が移行した部分（1層目）が体から剝がれる。2×10^{-8} cm/sなら1日で約20 μm，すなわち角層下層まで到達する。水分子は2×10^{-7}cm/sの皮膚透過性を示すので，数時間（2.4時間）で角層を透過することになる。最近ボールペン等で手にメモをとる学生をよく見かけるが，書いてすぐこの部分を擦ると文字は消される（ちなみに，これは角層上の皮脂によるものである）。しかし，しばらく(30分ほど)してから皮膚を擦っても文字は消えない。これは文字を形成する色素が角層中（おおよそ5層目以下）に滲入していくためである。これら色素の透過係数は3×10^{-7}cm/s以上であろうか。表2にこれら代表的物質の透過係数をまとめて示す。透過係数を使った皮膚透過速度の定量的概念の付与の手助けになれば幸いである。

もうひとつ，透過係数の具体的イメージに役立つのはどの程度の物質がどの程度の時間に吸収されるかということであろう。1 cm^2の断面積を有する皮膚に適用した物質（ただし物質は溶液として適用される）が1日に1％吸収された場合の透過係数は約1×10^{-7}cm/sであり，10％吸収された場合は約1×10^{-6}cm/sとなる。同様に10％吸収されるのに必要な時間が24時間なら約1×10^{-6} cm/sで，2.4時間なら約1×10^{-5}cm/sということもできる。

5. ナノ材料の性質について

ナノ材料の性質も皮膚透過性に影響する可能性がある。ナノ材料の性質の中で皮膚透過性に強く影響すると考えられる因子には，粒子径，形状（球形に近いかそれとも棒状に近いかなど），表面荷電（ゼータ電位），硬さ（粘性）などが挙げられる。

また，酸化チタンや酸化亜鉛の超微粒子を始めとして，一般的なナノ材料が皮膚にどの部分にまたどの程度侵入し滞留するかといった定量的データが少ない現状を考えると，まだこれらナノ材料の因子を十分議論することはできない。ただ，ニキビ治療薬としてadaparenのナノ粒子製剤Differinが日本でも上市されるようになった。また，粒子とは言えないが，リポソームや他の脂質集合体（液晶構造を有する脂質構造体を含む）・など高容積の脂質集合体の皮膚適用研究も進んできた。当然，これらの研究の延長上として酸化チタンや酸化亜鉛の超微粒子の皮膚浸透性や安全性検討も進んでくるものと思われる。

なお，生体に暴露されるナノ材料の安全性は，生体に入った後に蓄積されるものと分解・代謝・消失するものに分けて考える必要がある。アスベストやカーボンナノチューブは前者の代表である。また，リポソームなどは当然後者になる。紫外線散乱剤として用いられる酸化チタン超微粒子はどちらに分類されるか正しく評価してから安全性検討を開始する必要があろう[3]。

ナノ材料の安全性の評価は，いま始まったばかりである。今後の研究の進展を見守りたい。

参考文献

1）杉林堅次，*Fragrance Journal*，**35**（11），25～28（2007）
2）Bos J.D.，Meinardi M.M.，*Exp. Dermatol.*，**9**，165～169（2000）
3）K. Sugibayashi，H. Todo，E. Kimura，*J. Toxicol. Sci.*，**33**（3），293～298（2008）

Permeation Pathway of Macromolecules and Nanospheres through Skin

Hiroaki TODO,[a] Eriko KIMURA,[a] Hirotaka YASUNO,[a] Yoshihiro TOKUDOME,[a] Fumie HASHIMOTO,[a] Yoshiaki IKARASHI,[b] and Kenji SUGIBAYASHI*,[a,c]

[a] *Faculty of Pharmaceutical Sciences, Josai University;* [c] *Life Science Research Centre, Josai University; 1–1 Keyakidai, Sakado, Saitama 350–0295, Japan: and* [b] *National Institute of Health Sciences; 1–18–1 Kamiyoga, Setagaya-ku, Tokyo 158–8501, Japan.* Received February 15, 2010; accepted May 31, 2010; published online June 1, 2010

The permeation pathway of macromolecules and nanospheres through skin was evaluated using fluorescent isothiocyanate (FITC)-dextran (average MW, 4 kDa) (FD-4) and nanospheres (500 nm in diameter) in hairless rat abdominal skin and porcine ear skin as well as a three-dimensional cultured human skin model (cultured skin model). A low molecular hydrophilic compound, sodium fluorescein (FL) (MW, 376 Da), was used for comparison. FL penetrated the stratum corneum and permeated the viable epidermis of hairless rat skin, whereas less permeation of FL was observed through the cultured skin model, suggesting that the primary permeation pathway for the hydrophilic material may be skin appendages through the rat skin. A macromolecular compound, FD-4, was distributed through the hair follicles of the rat skin. In addition, nanospheres were detected in the hair follicles of porcine skin, although no skin permeation was detected. These findings suggest that appendage routes such as hair follicles can be a penetration pathway of macromolecules and nanospheres through skin.

Key words macromolecule; nanosphere; skin permeation pathway; transdermal drug delivery; hair follicle

Delivery of macromolecular compounds and nano-/microparticles has become more realistic due to the recent development of new tools and nanotechnologies for delivery enhancement.[1,2] The administration sites of such macromolecules and nano-/microparticles are supposed to be the mucosa, such as the gastrointestinal (GI) tract,[3] and ophthalmic, nasal and pulmonary[4] mucosa and skin.[5,6] Skin has been paid particular attention as an attractive administration site of these compounds because of its accessibility and easy application. Emulsion droplets, liposomes and other lipophilic carriers[7] containing small molecular active ingredients have already been investigated in the cosmetic field as well as therapeutic drug areas; however, the stratum corneum, the outermost layer of skin, has a primary function to protect the invasion and skin penetration of exogenous substances. Generally, only small molecular compounds less than 500 Da molecular weight are capable of significant passive permeation through the skin barrier (known as the 500 Dalton rule).[8] Thus, skin permeation of macromolecular compounds or nano-/microparticles is very difficult or impossible. Many reports have suggested that large molecules are likely to accumulate on the skin surface or appendages such as hair follicles.[9—12] Nevertheless, few reports have shown a quantitative approach for hair follicular penetration using quantitative skin permeation parameters.

Hairless rat and pig ear skins and three-dimensional cultured human skin model would be useful skin models with and without hair follicles, respectively, to clarify the contribution of hair follicles to skin permeation or the distribution of macromolecules and nanospheres.

In the present study, we selected fluorescent isothiocyanate (FITC)-dextran (average MW, 4 kDa) (FD-4) as a model macromolecular weight compound and 500 nm fluorescent polystyrene latex spheres as model nanospheres, and their potential for skin delivery was investigated by calculating skin permeation parameters or measuring the skin distribution of FD-4 and fluorescent polystyrene latex nanospheres in hairless rat abdominal skin and porcine ear skin as well as a three-dimensional cultured human skin model. Tables 1 and 2 summarize the model penetrant compounds and skin membranes used in this experiment. A low molecular hydrophilic compound, sodium fluorescein (FL) (MW 376 Da), was also used for comparison.

Theoretical Skin permeation kinetics is usually evaluated under an assumption that the skin consists of a single barrier membrane against drug permeation; however, generally, the drug-permeable membrane must be classed into three membranes: dissolution–diffusion membrane (Type 1 membrane), porous membrane (Type 2 membrane) and composite membrane (Type 3 membrane) of Type 1 and 2 membranes. Under the assumption that a single barrier of skin is one of these three membranes, the steady state skin permeation rate per unit application area, dQ/dt, is expressed using Fick's first law of diffusion as follows:

Type 1 membrane (dissolution–diffusion membrane)

$$\frac{dQ}{dt} = D \cdot \frac{K \cdot C_v}{L} = (KL)\left(\frac{D}{L^2}\right)C_v \tag{1}$$

Type 2 membrane (porous membrane)

$$\frac{dQ}{dt} = \frac{\varepsilon \cdot D_p}{\tau} \cdot \frac{C_v}{L} = (\varepsilon L)\left(\frac{D_p}{\tau L^2}\right)C_v \tag{2}$$

Type 3 membrane (composite membrane)

$$\frac{dQ}{dt} = (1-\varepsilon) \cdot D \cdot \frac{K \cdot C_v}{L} + \frac{\varepsilon \cdot D_p}{\tau} \cdot \frac{C_v}{L} = \left[\{(1-\varepsilon)KL\}\left(\frac{D}{L^2}\right) + (\varepsilon L)\left(\frac{D_p}{\tau L^2}\right)\right]C_v \tag{3}$$

where C_v is the initial concentration of the applied compound, D, K and L are diffusion coefficient, partition coefficient and barrier thickness of the membrane, respectively, and D_p, ε and τ are diffusion coefficients in water-filled pores, average fraction of diffusion area of pores, and tortuosity of the membrane, respectively. In examples 1 and 2, partition parameters and diffusion parameters of the pene-

* To whom correspondence should be addressed. e-mail: sugib@josai.ac.jp

trant are KL and DL^{-2} for the Type 1 membrane and εL and $D_p\tau^{-1}L^{-2}$ for the Type 2 membrane, respectively. The permeability coefficient, P, can be obtained as a product of the partition parameter and diffusion parameter. Diffusion lag time was obtained by dividing six by the diffusion parameter.

MATERIALS AND METHODS

Materials and Animals Both FL and FD-4 were obtained from Sigma-Aldrich Co., Ltd. (St. Louis, MO, U.S.A.). Fluorescent polystyrene latex nanospheres, Fluoresbrite® yellow green carboxylate microspheres (500 nm in average diameter), were purchased as model nanospheres from Polysciences, Inc. (Warrington, PA, U.S.A.). All other reagents and solvents were of reagent grade or HPLC grade, and used without further purification.

Male hairless rats (WBN/ILA-Ht, *ca.* 200—250 g) were supplied either from Life Science Research Center, Josai University (Sakado, Saitama, Japan) or Ishikawa Experimental Animal Laboratory (Fukaya, Saitama, Japan). Porcine ear skins were from Saitama Experimental Animal Laboratory (Sugito, Saitama, Japan). A three-dimensional cultured human skin model, Living Skin Equivalent-high (LSE-high), was obtained from Toyobo (Osaka, Japan).

Determination of *n*-Octanol–Water Partition Coefficient *n*-Octanol–water partition coefficient ($K_{o/w}$) of each fluorescent compound (FL or FD-4) was measured using distilled water–saturated *n*-octanol and *n*-octanol–saturated pH 7.4 phosphate buffered saline (PBS) at 32 °C. *n*-Octanol was added to the same volume of pH 7.4 PBS containing 10 mg/ml of each fluorescent, and the thoroughly mixed solution was equilibrated for 24 h. The aqueous phase was then analyzed using a fluorescence spectrophotometer (RF 5300PC; Shimadzu, Kyoto, Japan) at excitation and emission wavelengths of 490 and 520 nm, respectively. Logarithmic values of the partition coefficients are shown in Table 1.

***In Vitro* Skin Permeation Study** The skin permeation of FL and FD-4 was assessed using excised hairless rat abdominal skin and LSE-high. After the rats had been anesthetized by intraperitoneal injection of sodium pentobarbital (50 mg/kg), the abdominal skin was excised as described in our previous paper.[14] Stripped hairless rat skin was also used after removing the stratum corneum from the abdominal area by stripping 20 times with adhesive tape (Cellophane tape; Nichiban Co., Ltd., Tokyo, Japan). LSE-high was used after removing cultured skin pieces from the plastic insert with a knife. Each skin membrane was mounted in the side-by-side diffusion cell (effective diffusion area: 0.95 cm^2),[15,16] and 1.0 mM FL or 0.25 mM FD-4 (2.5 ml each) was applied to the stratum corneum side and the same volume of PBS was applied to the dermal side. Samples of 0.40 ml were taken periodically from the dermal side compartment, and then the same volume of the same solvent was added to keep the volume constant. FL or FD-4 concentration of each sample was determined using a fluorescence spectrophotometer, as explained above. The hairless rat skin and LSE-high surfaces were carefully rinsed with PBS several times to remove FL or FD-4 attached to the stratum corneum 6 h after starting the experiment. The obtained skin sample was embedded in Tissue-Tek® OTC compound (Miles, Inc., Elkhart, IN, U.S.A.) and stored at −80 °C until slicing.

Table 1. Physicochemical Properties of Model Compounds

Model compounds (abbreviation)	Molecular weight (Da)	Mean particle size or molecular radius	Log $K_{o/w}$ [a]
Sodium fluorescein (FL)	376	0.45 nm[13] (Stokes radius)	−0.615
FITC-dextran (FD-4)	4000	1.4 nm (Stokes radius)[13]	−0.773
Fluorescent polystyrene latex nanospheres (Fluoresbrite)	—	500 nm	—

a) $K_{o/w}$: *n*-octanol–water partition coefficient.

The skin permeation property of fluorescent polystyrene latex spheres (Fluoresbrite) was evaluated using excised hairless rat skin and excised porcine ear skin, which had been carefully shaved and the underlying excess fatty tissues removed from the dermis. LSE-high was also used to evaluate whether Fluoresbrite permeates the cultured skin. The obtained skin membranes were mounted in a Franz-type diffusion cell[14] (effective diffusion area: 1.77 cm^2). Then, 1.0 ml PBS-suspended solution containing Fluoresbrite (3.64×10^{10} particles/ml for 500 nm spheres) was applied to the stratum corneum surface, whereas 6.0 ml PBS was applied to the dermal side. The skin permeation test was performed at 32 °C over 12 h through hairless rat skin, porcine ear skin and LSE-high, while the receiver solution was continuously stirred with a star-head-type magnetic stirrer. The receiver solution was withdrawn 12 h after beginning the permeation experiment. The skins were then carefully rinsed with PBS several times to remove polystyrene spheres attached to the stratum corneum 12 h after starting the experiment. The obtained skin sample was embedded in Tissue-Tek® OTC compound (Miles, Inc., Elkhart, IN, U.S.A.) and stored at −80 °C until slicing.

All animal experiments were approved by the Institutional Animal Care and Use Committee of Josai University.

Evaluation of Skin Permeation Kinetics Steady-state flux was calculated by linear regression of the linear portion of normalized cumulative amount of penetrant permeated *versus* the time-curve (steady state; reached 4—6 h after starting the experiment), and the lag time was calculated from the intercept on the time axis by extrapolation from the steady state skin permeation profile. The normalized cumulative amount of penetrant permeated, Q_n, was calculated by dividing the cumulative amount permeated per unit area of skin by the initial concentration of the applied fluorescent compound in the donor compartment.[17] The permeation parameters were obtained by curve fitting the skin permeation data by Scheuplein's equation,[18] which comes from Fick's second law of diffusion. The least squares curve fitting method was performed using Microsoft® Excel Solver.[19] The calculation condition was 100 s for the calculation limit, 100 times for repeated calculation, 10^{-6} for accuracy, 5% basic tolerance and 10^{-3} for convergence. The pseudo-Newtonian method was used as an algorithm.

Sectioning of Hairless Rat Skin, Porcine Ear Skin and LSE-High Hairless rat skin, porcine ear skin and LSE-high embedded in Tissue-Tek® OTC compound were sequentially sliced with a cryostat (CM3050S; Leica, Wetzlar, Germany) to obtain horizontal and vertical 20 μm-thick sections. The prepared skin sections were observed with a fluorescence mi-

Table 2. Comparison of Skin Thickness and Presence or Absence of Hair Follicles in Several Skin Models

Skin model	Skin structure constitution	Stratum corneum thickness (μm)	Epidermis thickness (μm)	Whole skin thickness (mm)	Skin appendage	Relationship to human skin permeation
Hairless rat skin	Epidermis/dermis	15.4±3.3[20]	23.8±5.3[20]	0.86±0.06[20]	Yes	High
Pig skin	Epidermis/dermis	10.6±0.5	52.5±4.1	1.2±0.002	Yes	High
LSE-high	Epidermis/dermis	27.0±0.7	31.4±1.3	0.12±0.001	No	High

croscope (CK40; Olympus Corp., Tokyo, Japan).

Measurement of Thickness in LSE-High and Porcine Skin The thicknesses of the stratum corneum, epidermis, and whole skin in LSE-high and porcine skin were microscopically determined from microtomed sections after hematoxylin–eosin staining. Five good sections from each specimen were used to measure the stratum corneum, and whole skin thicknesses were measured by a light micrograph (IX71; Olympus Corp., Tokyo, Japan) and a calibrated ocular micrometer. The thickness of the epidermis was calculated by subtracting the stratum corneum thickness from the whole skin thickness. The thickness of hairless rat skin was cited from our previous paper.[20]

Observation of Skin Surface Shaved hairless rat and porcine ear skins were mounted with adhesive tape on a scanning microscopy (SEM) stage, and the skin surface was observed without coating by a low-vacuum SEM (S-3000N; Hitachi Ltd., Tokyo, Japan).

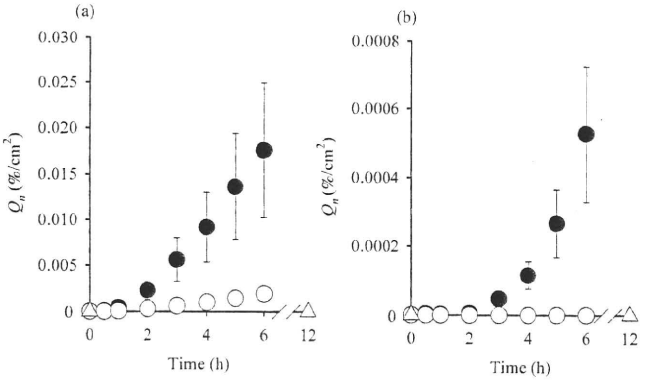

Fig. 1. Cumulative Amount of Hydrophilic Fluorescent Compounds, FL (●), FD-4 (○) and 500 nm Fluoresbrite (△) through Hairless Rat Skin (a) and LSE-High (b)

Normalized cumulative amount of the compounds permeating a percent per unit application area (%/cm^2)[17] was plotted on the vertical axis. Each data point represents the mean±S.E. of 3—4 experiments.

RESULTS

Many reports have shown that nano-/microspheres could not permeate the healthy stratum corneum.[21] In our study, therefore, the penetration pathway of hydrophilic fluorescent markers, FL and FD-4, was observed to evaluate the potential penetration of these mal-absorptive materials into skin and the delivery pathway through the skin barrier. The characteristics of model skin membranes (excised hairless rat skin, pig ear skin and LSE-high) are shown in Table 2. The stratum corneum in LSE-high was much thicker than the others. In addition, skin appendages such as sweat ducts and hair follicles could not be observed in LSE-high. Although many structural differences could be found between LSE-high and the others, and the permeation of several compounds (MW 122—236, $-1.5<\log K_{o/w}<2.1$) through LSE-high was about 10 times higher than through hairless rat and human skins, and the permeation rate through LSE-high showed a linear relationship to that through hairless rat and human skins.[14]

Figure 1a and b show the time course of the normalized cumulative amount of FL and FD-4 that permeated the unit area of excised hairless rat skin and LSE-high, respectively. In these experiments, 1.0 mM FL or 0.25 mM FD-4 (2.5 ml each) was applied to the skin surface to follow skin permeation. Interestingly, both fluorescent markers permeated hairless rat skin, whereas less permeation of FL and no permeation of FD-4 were observed through LSE-high. The Q_n of FL through hairless rat skin was 30-fold higher than through LSE-high.

The typical lag time and subsequent steady state permeation were observed for the permeation of both fluorescents through hairless rat skin. Permeability coefficients of FL and FD-4 were calculated by two methods using steady-state flux (observed value) and the curve fitting method (estimated value). These values are summarized in Table 3. The estimated vales were almost equal to the corresponding observed values and no significant differences appeared in hairless rat data. The calculated values of the permeability coefficient and Q_n of FL through LSE-high were about one-twelfth and one-thirtieth through hairless rat skin, respectively; furthermore, the lag time of FL through LSE-high (estimated value) was about three-fold of that through hairless rat skin. On the other hand, lag times of FL and FD-4 through hairless rat skin were almost the same as those through LSE-high.

Fluoresbrite was also applied to hairless rat skin and LSE-high. Although a Franz-type diffusion cell was used for measuring the skin permeation of Fluoresbrite, no permeation of the nanospheres was detected 12 h after starting the skin permeation experiment (see Fig. 1). No skin permeation was detected when Fluoresbrite was applied to porcine ear skin (data not shown).

Figure 2 shows fluorescent photographs illustrating the skin distribution of FL and FD-4 in hairless rat skin and LSE-high after topical application of these fluorescent markers. High-intensity FL was detected both in the stratum corneum and hair follicles of hairless rat (Fig. 2a), whereas FD-4 was mainly observed in the hair follicles (Fig. 2b). On the other hand, with LSE-high, FL was detected mostly in the stratum corneum and slightly in the viable epidermis (Fig. 2c) and FD-4 was found only on the skin surface (no skin penetration was observed for FD-4) (Fig. 2d). These results also suggest the high contribution of the transfollicular pathway to the transport of mal-absorptive hydrophilic compounds across the skin. In addition, this tendency was more

Table 3. Lag Time and Permeability Coefficients of FL and FD-4 through Excised Hairless Rat Skin or LSE-High

		FL		FD-4	
		Lag time (h)	Permeability coefficient (cm/s)	Lag time (h)	Permeability coefficient (cm/s)
Hairless rat	Estimated value[a)]	2.0±0.16	$(1.1\pm0.5)\times10^{-8}$	2.2±0.01	$(3.6\pm0.2)\times10^{-9}$
	Observed value[b)]	1.8±0.20	$(1.2\pm0.5)\times10^{-8}$	2.1±0.01	$(3.4\pm0.2)\times10^{-9}$
LSE-high	Estimated value[a)]	5.4±0.4	$(9.4\pm2.4)\times10^{-10}$	—	$\ll1.21\times10^{-10}$ [d)]
	Observed value[b)]	—[c)]	—[c)]	—[c)]	—[c)]

a) Estimated value was calculated by curve-fitting the time course of the cumulative amount of skin permeation of compounds using Scheuplein's equation.[25] *b*) Observed value was obtained by the slope of steady-state flux and time–axis intercept of the time course of the cumulative amount of skin permeation of compounds. *c*) No steady state permeation was obtained until 6 h in the skin permeation study. *d*) Estimated value was calculated from lower quantitative limit of FD-4 in receiver cell 6 h after skin permeation study.

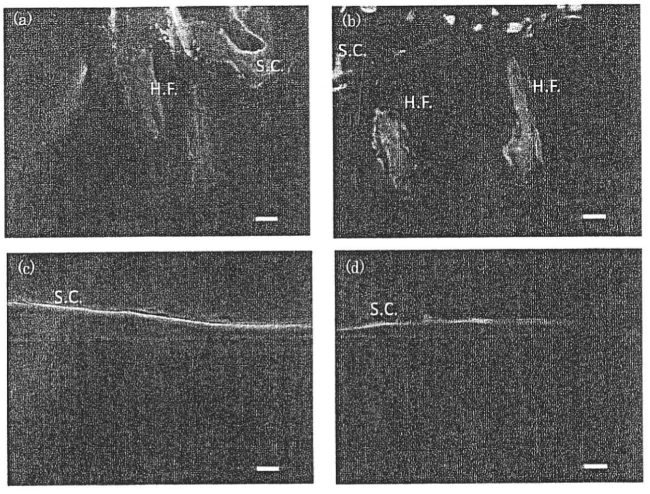

Fig. 2. Histological Observation of Hairless Rat Intact Skin (a, b) and LSE-High (c, d) after Application of FL (a, c) and FD-4 (b, d)

S.C.: Stratum corneum; H.F.: hair follicle. White bars=100 μm. (a, b): Fluorescence derived from FL or FD-4 was observed on the skin surface of skin and in hair follicles, (c, d): fluorescence derived from FL or FD-4 was observed in shallow areas or only on the surface, respectively, of LSE-high.

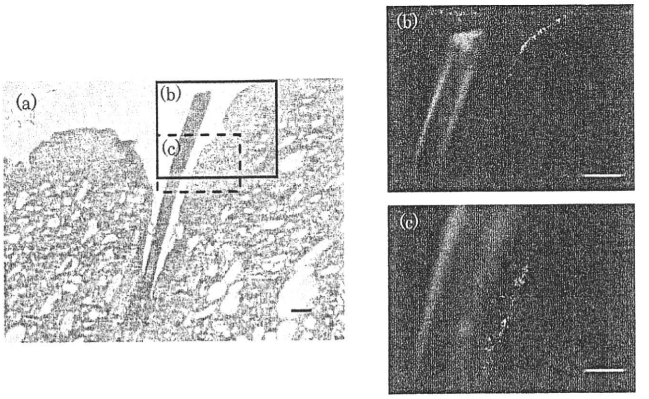

Fig. 3. Histological Observation of Excised Porcine Ear Skin 12 h after Application of 500 nm Fluoresbrite

a: Light micrograph of vertical slice. b and c: Fluorescent micrograph of area b and c in Fig. 3a. Bar=200 μm. (b, c): Fluoresbrite was observed in infundibulum of the hair follicle and surface of the hair shaft.

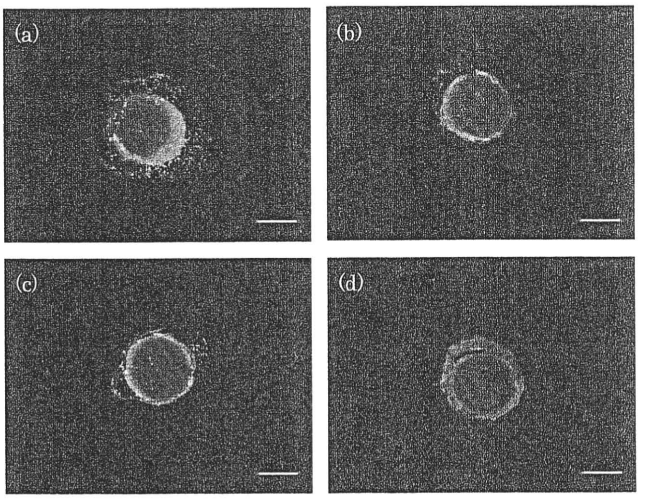

Fig. 4. Localization of 500 nm Fluoresbrite Penetrating the Hair Follicle

Fluorescence images (a—d) are horizontal slices at different depths from the skin surface of excised porcine ear skin 12 h after application of particles. a: *ca.* 20 μm, b: 40—60 μm, c: 80—100 μm, d: 200—220 μm. Bar=100 μm. (a): Fluoresbrite was detected on the surface of hair shaft and connective tissue in the follicle, (b, c): number of particles gradually decreased with an increase in depth from the skin surface, (d) only autofluorescence was observed.

marked when using the macromolecular compound. Thus, skin appendages such as hair follicles must be very important for the skin permeation of malabsorptive compounds.

Next, the skin distribution of Fluoresbrite (500 nm in diameter) was investigated after topical application to excised hairless rat skin, excised porcine ear skin and LSE-high. Nanospheres were detected only on the surface of the stratum corneum (data not shown) for hairless rat skin and LSE-high; therefore, a detailed observation was performed using excised porcine skin, since it has much larger hair follicles. Figure 3a shows a light microphotograph of porcine skin (vertical slice of hair follicle area) 12 h after the application of Fluoresbrite, and Figure 3b and c show fluorescent microphotographs of specific parts of the hair follicle area, as explained in Fig. 3a. Many nanospheres were found around the openings of the hair follicle, especially close to the epidermis side and around the hair shaft, as shown in Fig. 3b and c. The penetration depth of Fluoresbrite in the hair follicles was investigated by preparing horizontal slices of the hair follicle area of skin. The thickness of each skin section was adjusted to 20 μm. Figure 4 shows typical cross-section images of the hair follicle area from the skin surface (0—20 μm) to dermis side (200—220 μm) 12 h after application of Fluoresbrite to the excised porcine ear skin. In accordance with the photograph in Fig. 3, nanospheres could be detected in hair follicles, such as the surface of the hair shaft and connective tissue follicles, and the intensity due to nanospheres in the hair follicle gradually decreased with increasing pene-

tration depth; however, nanospheres could not be detected in connective tissue follicles below 200-μm depth from the skin surface. Only greenish-yellow autofluorescence derived from keratin and melanin was observed in Fig. 4d. This result clearly identified that the nanospheres were distributed or penetrated until about 100-μm depth, but did not penetrate as far as 200-μm depth from the skin surface 12 h after application. Thus, macromolecular compounds, such as FD-4 and nanospheres, are probably distributed or penetrate through the transfollicular pathway, although the extent is very marginal.

DISCUSSION

Three kinds of membranes are frequently utilized to describe the membrane permeation profiles of compounds, as explained in the theoretical section. In the dissolution–diffusion membrane (Type 1 membrane), compounds are dissolved and distributed into the membrane and then diffused in the homogeneous membrane. In the microporous membrane (Type 2 membrane), compounds are diffused across solvent (usually aqueous)-filled pores in the membrane. The third membrane (composite membrane) is the previous two membranes combined.

In the case of hairless rat and porcine skins, the stratum corneum and skin appendage may be the permeation pathway of compounds, especially for low molecular compounds ($\leq$500 Da). Thus, these animal skins would be assumed to be the third membrane. On the other hand, LSE-high would be classified as a dissolution–diffusion membrane, since three-dimensional cultured human skin model has no appendages, such as hair follicles and sweat ducts.

Although LSE-high is such a skin appendage-deficiency model, it was observed in our previous study[14] that logarithmic values of the permeability coefficient, log P, of seven drugs through LSE-high were fairly proportional to those through excised hairless rat, pig and human skins, and the partition parameters of LSE-high were almost the same as in other skins. For FL and FD-4 applied to LSE-high, low permeation and no permeation were observed in the present study, while permeation through hairless rat skin was observed. The permeability coefficient, P, of FD-4 through LSE-high was calculated from the lower quantitative limit of FD-4 in receiver solution (Table 3). The estimated value was about thirtieth of that of FD-4 through hairless rats. FL (pK_a 1: 4.32, pK_a 2: 6.5)[22] predominantly exists as an ionized form in pH 7.4 PBS, and FD-4 has a high molecular weight; therefore, the P-value of FL and FD-4 through LSE-high was much lower than through hairless rat skin.

The P-value is a product of the partition parameter (KL or εL) and diffusion parameter (DL^{-2} or $D_p\tau^{-1}L^{-2}$).[23] To clarify the differences of skin permeation profiles between hairless rat skin and LSE-high, the partition parameter and diffusion parameter were compared.

Table 4 shows the partition and diffusion parameters, which were calculated from curve-fitting the time course of the cumulative amount of FL and FD-4 permeating hairless rat skin and LSE-high. Interestingly, both parameters of LSE-high calculated from FL permeation were not the same as those of hairless rat skin. These differences might reflect the different permeation routes of FL between these skins.

Table 4. Comparison of Partition Parameter and Diffusion Parameter between Hairless Rat Skin and LSE-High

Compound	Membrane	Partition parameter (KL or εL) (cm)	Diffusion parameter (DL^{-2} or $D_p\tau^{-1}L^{-2}$) (s^{-1})
FL	Hairless rat	$(4.7\pm1.8)\times10^{-4}$	$(2.3\pm0.18)\times10^{-5}$
	LSE-high	$(1.1\pm0.31)\times10^{-4}$	$(8.6\pm0.75)\times10^{-6}$
FD-4	Hairless rat	$(1.7\pm0.13)\times10^{-4}$	$(2.0\pm0.06)\times10^{-5}$
	LSE-high	—	—

KL and DL^{-2} or εL and $D_p\tau^{-1}L^{-2}$ were calculated by curve-fitting the skin permeation profile of FL and FD-4 through hairless rat skin and LSE-high.

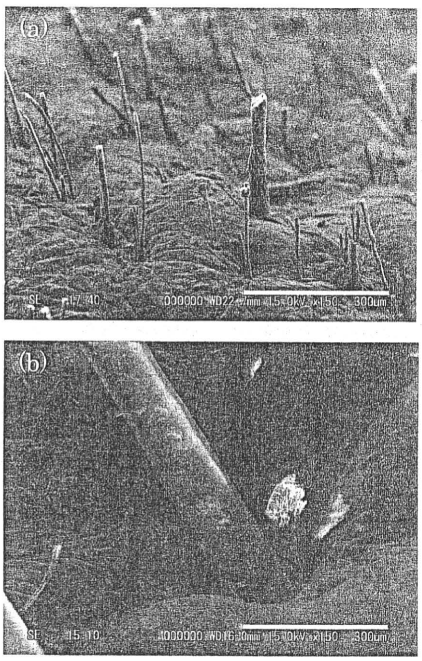

Fig. 5. SEM Observation of Hairless Rat Skin (a) and Porcine Ear Skin (b)

Bar=300 μm.

Increased partition and diffusion parameters of FL in hairless rat skin might mean that FL was mainly partitioned in pore routes and permeated the pore routes of skin; therefore, skin appendages, such as hair follicles, are the predominant permeation route of FL.

The diffusion parameters of FL and FD-4 in hairless rat skin showed almost the same value due to the slight difference in the cubic root of the molecular weight of these compounds, because the diffusion coefficient is proportional to the reciprocal of the cubic root, which is given by the Stokes–Einstein equation. Therefore, FL and FD-4 must permeate through almost the same permeation pathway of skin. On the other hand, the partition parameter of FD-4 was about one-third that of FL, indicating that FD-4 permeated skin through a more restricted pathway, such as hair follicles, than the FL pathway. In addition to this assumption, the present fluorescence images strongly supported the skin appendage route as a useful pathway for skin permeation and/or the distribution of such macromolecular compounds.

Fluoresbrite did not permeate hairless rat skin or LSE-high. Thus, porcine skin was selected to observe its skin distribution because the pores of hair follicles in porcine skin

are larger than in hairless rat skin (see Fig. 5). Fluoresbrite was especially observed in the infundibulum of hair follicles of porcine skin and no spheres were observed more than 100-μm depth from the skin surface (Fig. 4). It is reasonable that Fluoresbrite was detected only in the hair follicle because even FD-4, having a smaller molecular radius than nanospheres, was mainly detected in hair follicles.

This indicated that hair follicles are expected to be a useful pathway, not only for macromolecular compounds, but also nanospheres, through the skin barrier. Scheuplein[18] reported that the contribution of the transappendage route to the skin permeation of low molecular compounds must be very low, although the transfollicular pathway would play a very important role in the early stage of skin permeation and distribution. This is because the skin appendage area is only 0.1% of the total skin surface area.[18,24] Further study is necessary to fully elucidate the contribution of hair follicles to the skin permeation or distribution of hydrophilic compounds and nano-/microspheres. This contribution of hair follicles can be assessed using skin permeation parameters, such as $\varepsilon \cdot L$ and $D/\tau \cdot L^2$ as above.

CONCLUSION

The present study revealed that important role of hair follicles as a permeation pathway or distribution pathway for hydrophilic compounds and nanospheres. Although not only skin features, such as hair density and follicle size, but also physicochemical properties, such as molecular size and *n*-octanol/water partition coefficient of compounds, affect their transfollicular permeation,[25] analysis of the hair follicle contribution to the overall skin permeation of compounds using permeation parameters will help to understand efficient compound targeting of hair follicles.

Acknowledgement This study was supported by a Grant-in-Aid for Scientific Research (H20-iyaku-ippan-001) from the Ministry of Health, Labor, and Welfare, Japan.

REFERENCES

1) Ravi Kumar M. N., *J. Pharm. Pharm. Sci.*, **3**, 234—258 (2000).
2) Bilati U., Allemann E., Doelker E., *Eur. J. Pharm. Biopharm.*, **59**, 375—388 (2005).
3) Takeuchi H., Matsui Y., Sugihara H., Yamamoto H., Kawashima Y., *Int. J. Pharm.*, **303**, 160—170 (2005).
4) Todo H., Iida K., Okamoto H., Danjo K., *J. Pharm. Sci.*, **92**, 2475—2486 (2003).
5) Alvarez-Roman R., Naik A., Kalia Y. N., Guy R. H., Fessi H., *J. Controlled Release*, **99**, 53—62 (2004).
6) Almeida A. J., Souto E., *Adv. Drug Deliv. Rev.*, **59**, 478—490 (2007).
7) Honeywell-Nguyen P. L., Wouter Groenink H. W., Bouwstra J. A., *J. Liposome Res.*, **16**, 273—280 (2006).
8) Bos J. D., Meinardi M. M., *Exp. Dermatol.*, **9**, 165—169 (2000).
9) Lademann J., Weigmann H., Rickmeyer C., Barthelmes H., Schaefer H., Mueller G., Sterry W., *Skin Pharmacol. Appl. Skin Physiol.*, **12**, 247—256 (1999).
10) Toll R., Jacobi U., Richter H., Lademann J., Schaefer H., Blume-Peytavi U., *J. Invest. Dermatol.*, **123**, 168—176 (2004).
11) Trauer S., Patzelt A., Otberg N., Knorr F., Rozycki C., Balizs G., Buttemeyer R., Linscheid M., Liebsch M., Lademann J., *Br. J. Clin. Pharmacol.*, **68**, 181—186 (2009).
12) Teichmann A., Jacobi U., Ossadnik M., Richter H., Koch S., Sterry W., Lademann J., *J. Invest. Dermatol.*, **125**, 264—269 (2005).
13) Mota M. C., Carvalho P., Ramalho J., Leite E., *Int. Ophthalmol.*, **15**, 321—326 (1991).
14) Watanabe T., Hasegawa T., Takahashi H., Ishibashi T., Takayama K., Sugibayashi K., *Altern. Animal Test Experiment.*, **8**, 1—14 (2001).
15) Okumura M., Sugibayashi K., Ogawa K., Morimoto Y., *Chem. Pharm. Bull.*, **37**, 1404—1406 (1989).
16) Obata Y., Takayama K., Maitani Y., Machida Y., Nagai T., *Biol. Pharm. Bull.*, **16**, 312—314 (1993).
17) Sugibayashi K., Hosoya K., Morimoto Y., Higuchi W. I., *J. Pharm. Pharmacol.*, **37**, 578—580 (1985).
18) Scheuplein R. J., *J. Invest. Dermatol.*, **48**, 79—88 (1967).
19) Sugibayashi K., Hayashi T., Matsumoto K., Hasegawa T., *Drug Metab. Pharmacokinet.*, **19**, 352—362 (2004).
20) Sato K., Sugibayashi K., Morimoto Y., *J. Pharm. Sci.*, **80**, 104—107 (1991).
21) Scientific Committee on Consumer Product, "Opinion on Safety on Nanomaterials in Cosmetic Products," 2007.
22) Lauer A. C., Lieb L. M., Ramachandran C., Flynn G. L., Weiner N. D., *Pharm. Res.*, **12**, 179—186 (1995).
23) Okamoto H., Yamashita F., Saito K., Hashida M., *Pharm. Res.*, **6**, 931—937 (1989).
24) Ogiso T., Shiraki T., Okajima K., Tanino T., Iwaki M., Wada T., *J. Drug Target*, **10**, 369—378 (2002).
25) Knorr F., Lademann J., Patzelt A., Sterry W., Blume-Peytavi U., Vogt A., *Eur. J. Pharm. Biopharm.*, **71**, 173—180 (2009).